Monatshefte für Chemie 132, 1477–1492 (2001)

Monatshefte für Chemie
Chemical Monthly

Copper(II)-Catalyzed Decomposition of Hydrogen Peroxide: Catalyst Activation by Halide Ions

Joaquin F. Perez-Benito*

Departamento de Quimica Fisica, Facultad de Quimica, Universidad de Barcelona, E-08028 Barcelona, Spain

Summary. The catalytic action of Cu(II) on the decomposition of H_2O_2 in near-neutrality aqueous solutions is activated by halide ions. The activation energies amount to 113±7 (parent reaction) and 69.9±1.4 (chloride-activated reaction) $kJ \cdot mol^{-1}$. Free-radical chain mechanisms are proposed for both the parent reaction and the halide-activated reaction. The catalyst activation caused by halide ions is explained in terms of coordination of halide ligands by both Cu(II) and Cu(I), the coordination causing a higher stabilization of Cu(I) than of Cu(II). At low concentrations, Br^- causes an inhibition of the $Cu(II)/H_2O_2$ reaction. This is explained in terms of an increase of the rate of termination of the chain reaction due to the scavenging effect of OH radicals caused by Br^-.

Keywords. Catalysis; Copper(II); Hydrogen peroxide; Kinetics; Mechanism.

Introduction

The intracellular decomposition of hydrogen peroxide catalyzed by transition metal ions is thought to be involved (probably *via* a free-radical mechanism) in aging and carcinogenesis [1–3]. Presumably, mitochondrial *DNA* might be a prime target for the free-radical oxidative attack [4–7]. In particular, copper is the third-most abundant transition metal in the human body (after iron and zinc) [8] and is essential for life [9], since it is required in low concentration for the formation of important enzymes [10–13]. As one of the chemical constituents of cell nuclei it has been proposed to play an essential role in the structure and function of chromosomes [14]. Hence, most vitamin-mineral combined dietary supplements include Cu(II). However, Cu(II) is toxic at high concentrations, and its interaction with hydrogen peroxide might be at least partially responsible for this [15, 16].

In this paper, the results of a kinetic study on the decomposition of hydrogen peroxide catalyzed by Cu(II) at near-physiological *pH* are reported.

* E-mail: j.perez@qf.ub.es

Results and Discussion

Determination of kinetic data

The first part of the kinetic plots was fitted by the linear least-squares method to Eq. (1) where V is the volume of $KMnO_4$ solution required to titrate the aliquot extracted at time t (Fig. 1). The initial rate was obtained according to Eq. (2).

$$\ln V = a + bt \tag{1}$$

$$v_0 = -\left(\frac{\mathrm{d}[H_2O_2]}{\mathrm{d}t}\right)_{t=0} = -b[H_2O_2]_0 \tag{2}$$

All experiments were performed twice. In total, 632 kinetic runs (each involving 10 permanganate titrations) were done. The typical standard deviation of the initial rate was $\pm 3\%$.

Formation of a Cu(II)-phosphate complex

It has been reported that high phosphate concentrations inhibit the formation of a *DNA*-Cu(I) complex induced by Cu(II)-glutathione mixtures, and this effect has been attributed to the formation of a Cu(II)-phosphate complex [14]. In the present work, some evidences of complexation of Cu(II) by phosphate ions were obtained: (*i*) $[Cu(H_2O)_6]^{2+}$ shows an absorption band at 810 nm, and the intensity of this band increases in the presence of phosphate; (*ii*) by difference spectroscopy, using

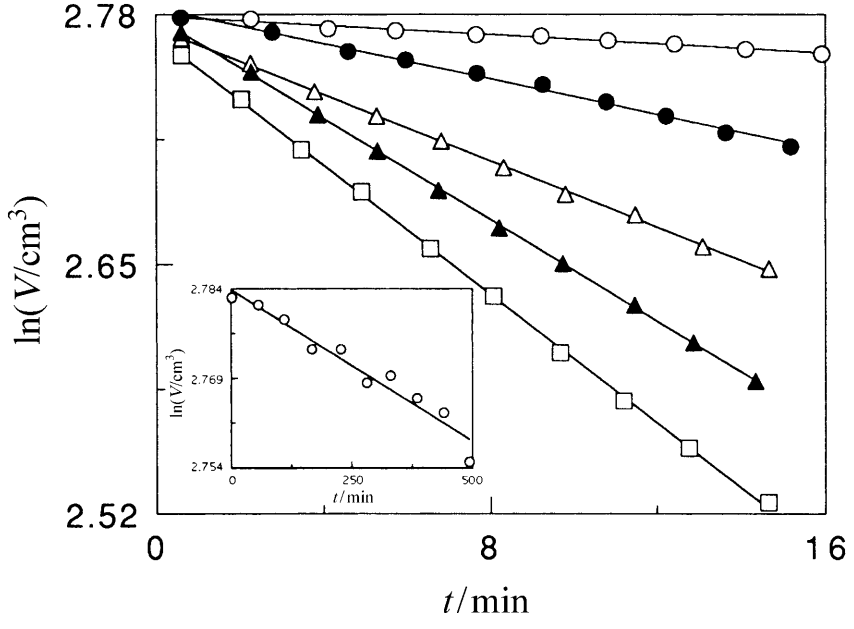

Fig. 1. Kinetic plots at various chloride ion concentrations and constant ionic strength ($[KCl] + [KNO_3] = 2.64\,M$); $[H_2O_2]_0 = 9.79 \times 10^{-2}\,M$, $[CuSO_4] = 1.20 \times 10^{-5}\,M$, $[KH_2PO_4] = [K_2HPO_4] = 1.20 \times 10^{-2}\,M$, $pH = 6.33 \pm 0.02$, $T = 25.0°C$; $[KCl] = 0.00$ (inset), 0.30 (empty circles), 0.90 (filled circles), 1.50 (empty triangles), 2.10 (filled triangles), and 2.64 (squares) M

a solution of $[Cu(H_2O)_6]^{2+}$ as reference, it was possible to detect an absorption band corresponding to a Cu(II)-phosphate complex ($\lambda_{max} = 237$ nm).

From the increase of the absorbance at 237 nm with increasing total phosphate concentration ($[H_3PO_4] + [KH_2PO_4]$) it could be inferred that, assuming the formula $[Cu(H_2PO_4)(H_2O)_5]^{+}$ for the complex, its formation constant from $[Cu(H_2O)_6]^{2+}$ and $H_2PO_4^-$ would be expected in the interval $0.05\,M^{-1} < K_f < 1\,M^{-1}$. A more precise determination of K_f was precluded by precipitation occurring at high phosphate concentrations. Since precipitation was favoured by high *pH* values the equilibrium measurements could only be carried out under acidic conditions (H_3PO_4–KH_2PO_4 mixtures). An increase of the intensity of the band at 237 nm with increasing *pH* seemed to indicate that the ligand bound to Cu(II) was $H_2PO_4^-$ rather than H_3PO_4.

Kinetic data of the parent reaction

In the absence of halide ions, the initial rate increased as the initial concentration of hydrogen peroxide increased (Table 1), yielding an apparent kinetic order of 1.87±0.07 for the reactant. The dependence of the initial rate on the concentration of Cu(II) varied notably with the experimental conditions. Over a large range of catalyst concentration, the v_0 *vs.* [Cu(II)] plots showed a definite (either upward-concave or downward-concave) curvature (Fig. 2), although at low catalyst concentrations almost linear plots were obtained (Fig. 2, inset).

At constant ionic strength and *pH*, the initial rate decreased as the total concentration of buffer ($[KH_2PO_4] + [K_2HPO_4]$) increased (Table 2). Keeping both ionic strength and total buffer concentration constant, the initial rate increased with increasing *pH* (Table 3), and the kinetic order of OH^- was near unity, the slope of a log v_0 *vs. pH* plot being 0.96±0.03. The initial rate *vs.* temperature data (Table 4) yielded a rather high activation energy of $113 \pm 7\,kJ \cdot mol^{-1}$.

Addition of different electrolytes caused either a decrease (KNO_3 and $NaClO_4$) or an increase (KCl) of the initial rate (Fig. 3). In all three cases the *pH* decreased due to an increase of the buffer equilibrium constant (for $H_2PO_4^- \rightleftarrows HPO_4^{2-} + H^+$) with increasing ionic strength. For both KNO_3 and $NaClO_4$ the decrease of the initial rate could be ascribed to the decrease of the *pH* caused by their addition, because the log v_0 *vs. pH* plots corresponding to variable ionic strength (by changing the concentrations of either KNO_3 or $NaClO_4$) and to constant ionic strength (by

Table 1. Dependence of the initial rate on the initial concentration of hydrogen peroxide in the absence of halide ions[a]

$[H_2O_2]_0 / M$	$v_0 / 10^{-6} M \cdot s^{-1}$
0.098	0.08±0.01
0.196	0.36±0.03
0.294	0.68±0.02
0.392	1.21±0.01
0.489	1.66±0.08

[a] $[CuSO_4] = 1.20 \times 10^{-5} M$, $[KH_2PO_4] = [K_2HPO_4] = 1.20 \times 10^{-2} M$, ionic strength: 2.64 *M* (KNO_3), *pH* = 6.30±0.04, 25.0°C

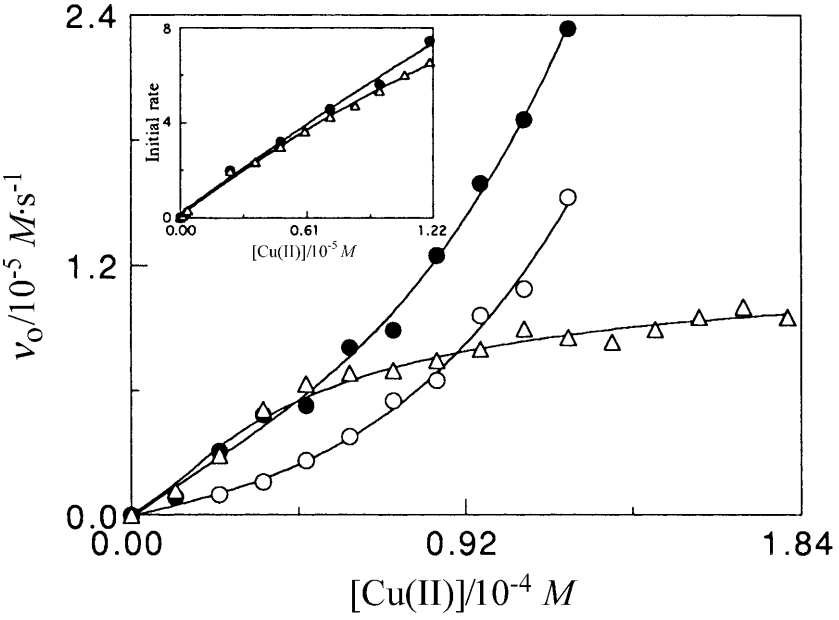

Fig. 2. Dependence of the initial rate on the concentration of $CuSO_4$; main figure: $[H_2O_2]_0 = 0.196$ (empty circles) and 0.392 (filled circles and triangles) M, $[KH_2PO_4] = [K_2HPO_4] = 1.20$ (triangles) and 6.00 (empty and filled circles) $\times 10^{-2}\,M$, $pH = 6.31 \pm 0.02$ (triangles) and 6.70 ± 0.01 (empty and filled circles), $[KNO_3] = 0$ (empty and filled circles) and 1.80 (triangles) M, 25.0°C; inset: initial rate in 10^{-7} (circles, $[KNO_3] = 2.64\,M$) or 10^{-5} (triangles, $[KCl] = 2.10\,M$) $M \cdot s^{-1}$ at $[H_2O_2]_0 = 0.392\,M$, $[KH_2PO_4] = [K_2HPO_4] = 1.20 \times 10^{-2}\,M$, $pH = 6.16 \pm 0.02$ (circles) and 6.26 ± 0.01 (triangles), 25.0°C

Table 2. Dependence of the initial rate on the total concentration of buffer in the absence of halide ions[a]

$[Buffer]_T/10^{-2}\,M$	$v_0/10^{-6}\,M\cdot s^{-1}$
2.40	1.27±0.01
3.60	0.97±0.07
4.80	0.91±0.01
6.00	0.89±0.01
7.20	0.76±0.03

[a] $[H_2O_2]_0 = 0.392\,M$, $[CuSO_4] = 1.20 \times 10^{-5}\,M$, $[KH_2PO_4] = [K_2HPO_4]$, ionic strength: $2.64\,M$ (KNO_3), $pH = 6.30 \pm 0.02$, 25.0°C

Table 3. Dependence of the initial rate on the pH in the absence of halide ions[a]

pH	$v_0/10^{-6}\,M\cdot s^{-1}$
6.16	0.20±0.01
6.32	0.30±0.02
6.51	0.41±0.01
6.74	0.74±0.01
7.04	1.40±0.02

[a] $[H_2O_2]_0 = 0.392\,M$, $[CuSO_4] = 2.40 \times 10^{-6}\,M$, $[KH_2PO_4] + [K_2HPO_4] = 2.40 \times 10^{-2}\,M$, ionic strength: $2.64\,M$ (KNO_3), 25.0°C

Table 4. Dependence of the initial rate on the temperature in the absence of halide ions[a]

$T/°C$	$v_0/10^{-6} M \cdot s^{-1}$
16.5	0.27±0.03
20.5	0.48±0.02
25.1	1.27±0.01
29.9	2.53±0.09
35.2	4.23±0.13

[a] $[H_2O_2]_0 = 0.392\,M$, $[CuSO_4] = 1.20 \times 10^{-5}\,M$, $[KH_2PO_4] = [K_2HPO_4] = 1.20 \times 10^{-2}\,M$, ionic strength: $2.64\,M$ (KNO_3), $pH = 6.26 \pm 0.02$

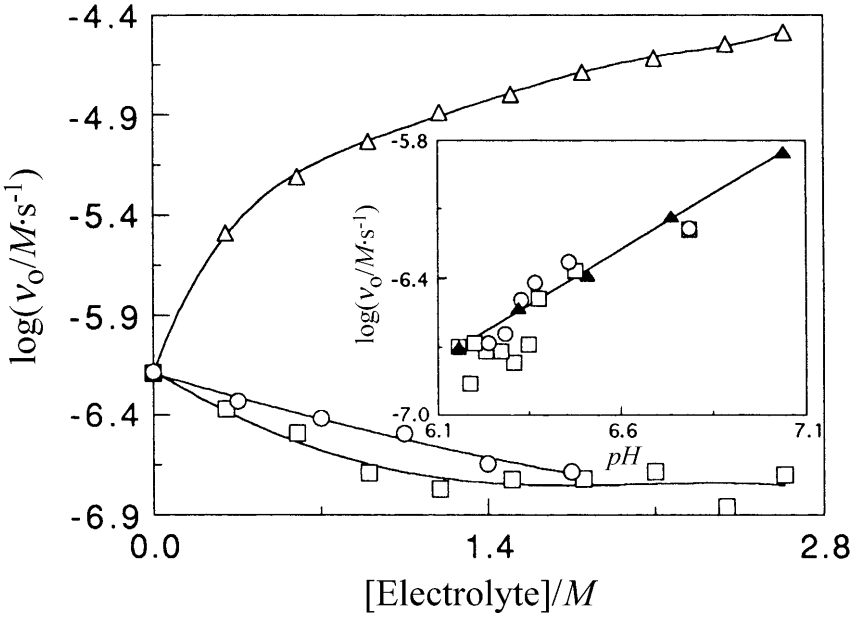

Fig. 3. Dependence of the logarithm of the initial rate on the concentrations of KNO_3 (squares), $NaClO_4$ (circles), and KCl (empty triangles) at $[H_2O_2]_0 = 0.392\,M$, $[CuSO_4] = 2.40 \times 20^{-6}\,M$, $[KH_2PO_4] = [K_2HPO_4] = 1.20 \times 10^{-2}\,M$, and 25.0°C; inset: dependence of the logarithm of the initial rate on the *pH* at variable $[KNO_3]$ (squares), $[NaClO_4]$ (circles), or components of the buffer (keeping $[KH_2PO_4] + [K_2HPO_4] = 2.40 \times 10^{-2}\,M$ and $[KNO_3] = 2.64\,M$, filled triangles)

changing the concentrations of the buffer components in the presence of a large excess of KNO_3) were rather consistent (Fig. 3, inset). Thus, both KNO_3 and $NaClO_4$ behaved as inert electrolytes, and the ionic strength had little (if any) effect on the initial rate. On the contrary, KCl had a specific enhancing effect on the rate of the decomposition of H_2O_2 catalyzed by Cu(II).

Kinetic data for the chloride-activated reaction

The effect of KCl on the reaction was studied at constant ionic strength using KNO_3 as inert (bottom) electrolyte. The initial rate increased with increasing concentration of KCl, and the plots were reasonably linear (Figs. 4–8). The slopes of the v_0 *vs.* [KCl] plots increased with increasing initial concentration of H_2O_2,

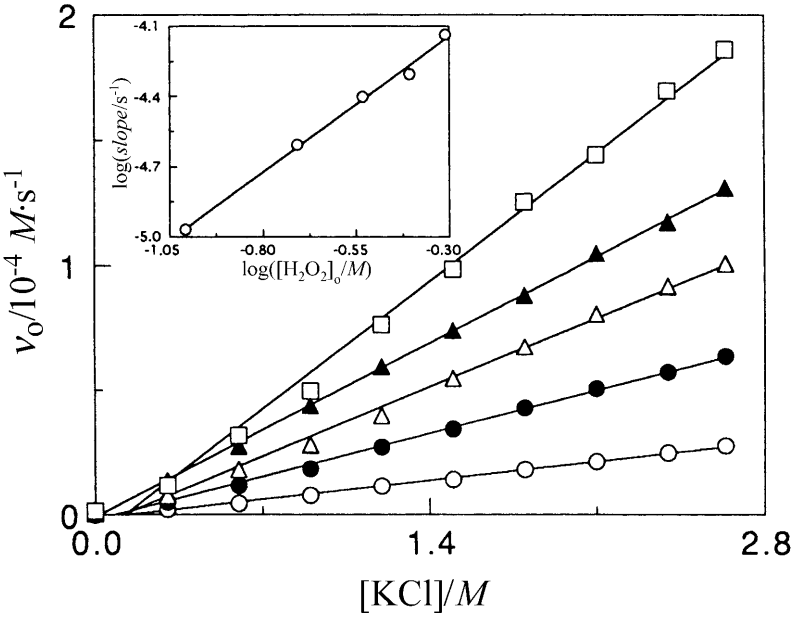

Fig. 4. Dependence of the initial rate on the concentration of KCl at various reactant initial concentrations and constant ionic strength ([KCl] + [KNO_3] = 2.64 *M*); [$CuSO_4$] = 1.20×10^{-5} *M*, [KH_2PO_4] = [K_2HPO_4] = 1.20×10^{-2} *M*, *pH* = 6.28±0.04, 25.0°C; [H_2O_2]$_0$ = 0.098 (empty circles), 0.196 (filled circles), 0.294 (empty triangles), 0.392 (filled triangles), and 0.489 (squares) *M*; inset: double-logarithmic dependence of the slope of each v_0 *vs.* [KCl] plot on the initial concentration of H_2O_2

yielding an apparent kinetic order of 1.16±0.05 (Fig. 4, inset) for the reactant in the chloride-activated reaction which is considerably lower than the value for the parent reaction under the same experimental conditions (1.87±0.07). The slopes of the v_0 *vs.* [KCl] plots increased linearly with increasing concentration of Cu(II) (Fig. 5, inset). The fact that the latter plot had a zero intercept indicated that Cl^- did not catalyze the decomposition of H_2O_2 in the absence of Cu(II) under the experimental conditions (*pH* near neutrality) of this study, although catalysis is known to occur in acidic solutions [17].

The slope of each v_0 *vs.* [KCl] plot decreased with increasing total concentration of buffer and increased with increasing *pH* according to Eqs. (3) and (4), so that the reciprocal of the slope increased linearly with either increasing total concentration of buffer (Fig. 6, inset) or increasing concentration of hydrogen ion (Fig. 7, inset). The fitting parameters were $a' = (2.02\pm0.10) \times 10^{-6}\ M\cdot s^{-1}$, $b' = (1.8\pm0.4) \times 10^{-2}\ M$, $a'' = (1.33\pm0.03) \times 10^{-11}\ M\cdot s^{-1}$, and $b'' = (6.2\pm0.2) \times 10^{-7}\ M$. The parent reaction was much more sensitive to an increase of the *pH* than the chloride-activated reaction; an increase of the *pH* from 6.16 to 7.04 resulted in a 7-fold increase of the rate in the former case (Table 3), but only in a less than 2-fold increase in the latter.

$$slope = \frac{a'}{[\text{Buffer}]_T + b'} \tag{3}$$

$$slope = \frac{a''}{[H^+] + b''} \tag{4}$$

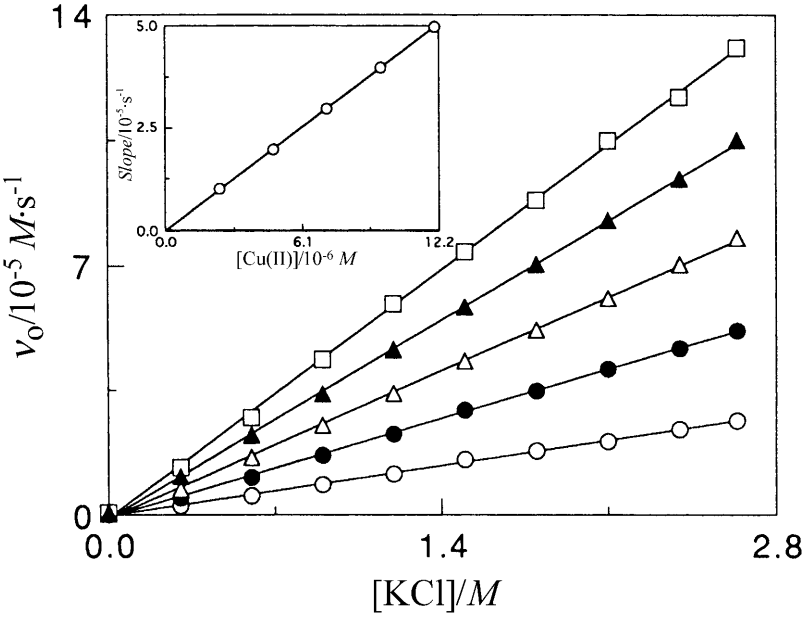

Fig. 5. Dependence of the initial rate on the concentration of KCl at various catalyst concentrations and constant ionic strength ($[KCl] + [KNO_3] = 2.64\,M$); $[H_2O_2]_0 = 0.392\,M$, $[KH_2PO_4] = [K_2HPO_4] = 1.20 \times 10^{-2}\,M$, $pH = 6.15 \pm 0.02$, 25.0°C; $[CuSO_4] = 2.41$ (empty circles), 4.81 (filled circles), 7.22 (empty triangles), 9.62 (filled triangles), and 12.0 (squares) $\times\ 10^{-6}\,M$; inset: dependence of the slope of each v_0 *vs.* [KCl] plot on the concentration of $CuSO_4$

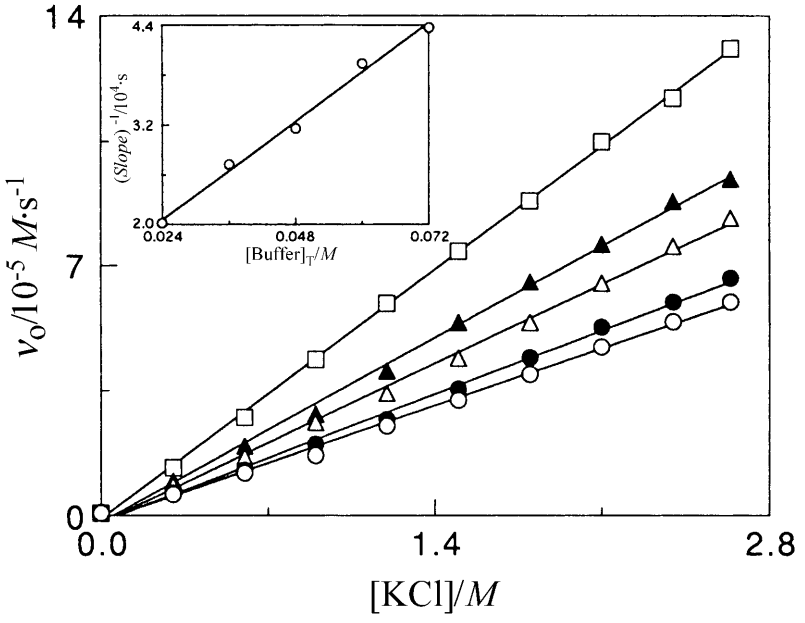

Fig. 6. Dependence of the initial rate on the concentration of KCl at various total concentrations of buffer and constant ionic strength ($[KCl] + [KNO_3] = 2.64\,M$); $[H_2O_2]_0 = 0.392\,M$, $[CuSO_4] = 1.20 \times 10^{-5}\,M$, $[KH_2PO_4] = [K_2HPO_4]$, $pH = 6.23 \pm 0.04$, 25.0°C; $[Buffer]_T = 0.024$ (squares), 0.036 (filled triangles), 0.048 (empty triangles), 0.060 (filled circles), and 0.072 (empty circles); inset: dependence of the reciprocal of the slope of each v_0 *vs.* [KCl] plot on the total concentration of buffer

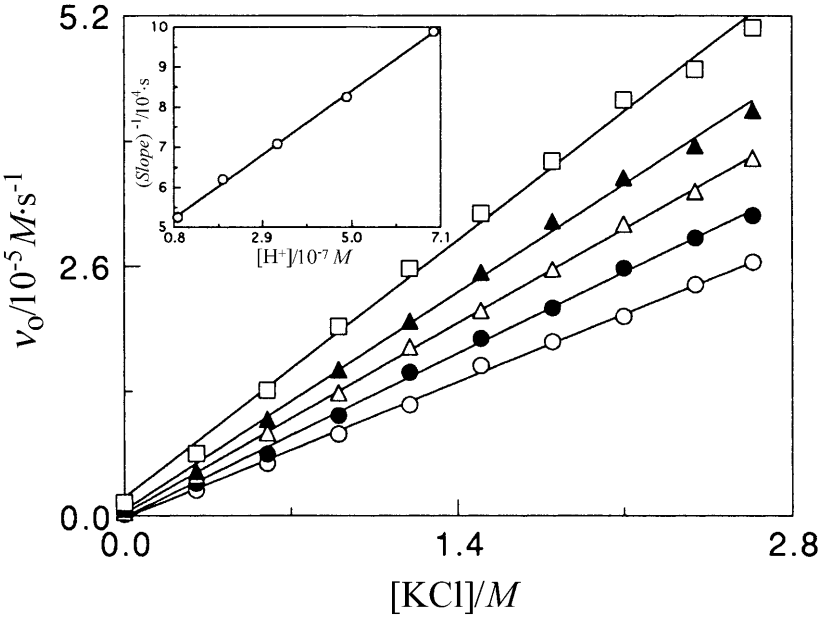

Fig. 7. Dependence of the initial rate on the concentration of KCl at various *pH* values and constant ionic strength ($[KCl] + [KNO_3] = 2.64\,M$); $[H_2O_2]_0 = 0.392\,M$, $[CuSO_4] = 2.40 \times 10^{-6}\,M$, $[KH_2PO_4] + [K_2HPO_4] = 2.40 \times 10^{-2}\,M$, 25.0°C; $pH = 6.16 \pm 0.03$ (empty circles), 6.31 ± 0.02 (filled circles), 6.49 ± 0.02 (empty triangles), 6.71 ± 0.02 (filled triangles), and 7.05 ± 0.02 (squares); inset: dependence of the reciprocal of the slope of each v_0 *vs.* [KCl] plot on the concentration of hydrogen ions

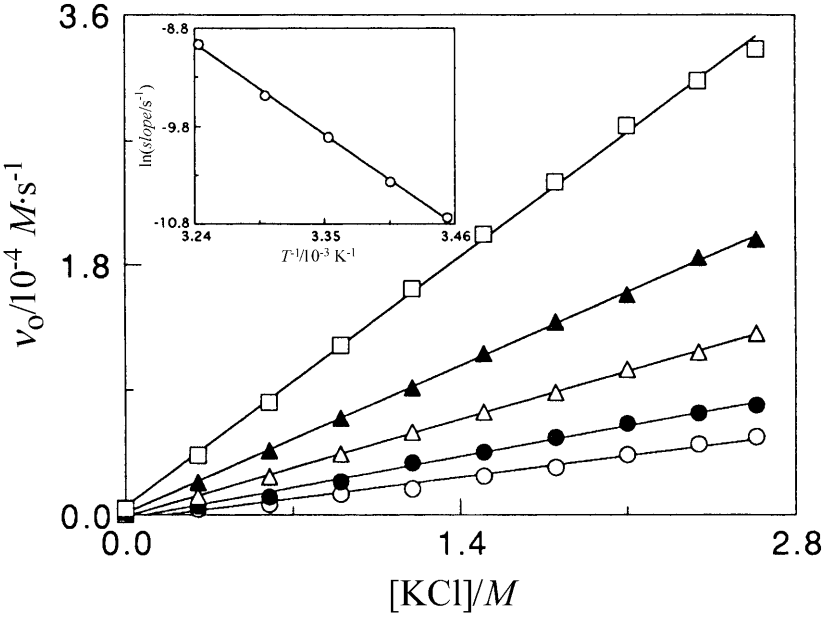

Fig. 8. Dependence of the initial rate on the concentration of KCl at various temperatures and constant ionic strength ($[KCl] + [KNO_3] = 2.64\,M$); $[H_2O_2]_0 = 0.392\,M$, $[CuSO_4] = 1.20 \times 10^{-5}\,M$, $[KH_2PO_4] = [K_2HPO_4] = 1.20 \times 10^{-2}\,M$, $pH = 6.23 \pm 0.04$; temperatures: 16.5 (empty circles), 20.5 (filled circles), 25.1 (empty triangles), 29.9 (filled triangles), and 35.2 (squares)°C; inset: *Arrhenius* plot for the slopes of the v_0 *vs.* [KCl] plots

Table 5. Initial rates for the chloride activated reaction at various ionic strengths[a]

$[KNO_3]/M$	ionic strength/M	$v_0/10^{-5} M \cdot s^{-1}$
0.000	2.10	1.99±0.07
0.060	2.16	2.06±0.01
0.120	2.22	2.03±0.06
0.180	2.28	2.09±0.03
0.240	2.34	2.00±0.04

[a] $[H_2O_2]_0 = 0.392\,M$, $[CuSO_4] = 2.40 \times 10^{-6}\,M$, $[KCl] = 2.10\,M$, $[KH_2PO_4] = [K_2HPO_4] = 1.20 \times 10^{-2}\,M$, $pH = 6.23 \pm 0.01$, 25.0°C

The slopes of the v_0 *vs.* [KCl] plots obeyed *Arrhenius*' law (Fig. 8, inset), and the associated activation energy was $69.9 \pm 1.4\,kJ \cdot mol^{-1}$, much lower than that of the parent reaction ($113 \pm 7\,kJ \cdot mol^{-1}$). The rate of the chloride-activated reaction was not appreciably affected by the addition of KNO_3, at least in the range of the high ionic strengths studied (Table 5).

Comparison with other halides

The initial rate did not increase linearly with the concentration of KBr (as in the case of KCl). Instead, the v_0 *vs.* [KBr] plot was slightly sigmoidal, showing an upward-concave curvature at low KBr concentration and a downward-concave curvature at high KBr concentration. A comparison of the initial rate data obtained in the presence of KCl with those obtained in the presence of KBr under the same

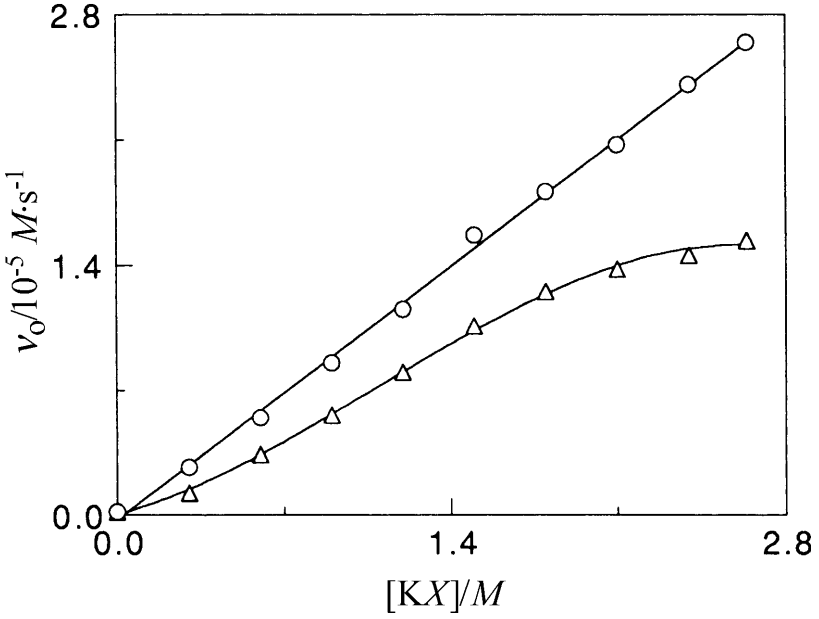

Fig. 9. Dependence of the initial rate on the concentrations of KCl (circles) and KBr (triangles) at constant ionic strength ($[KX] + [KNO_3] = 2.64\,M$); $[H_2O_2]_0 = 0.392\,M$, $[CuSO_4] = 2.40 \times 10^{-6}\,M$, $[KH_2PO_4] = [K_2HPO_4] = 1.20 \times 10^{-2}\,M$, $pH = 6.14 \pm 0.03$, 25.0°C

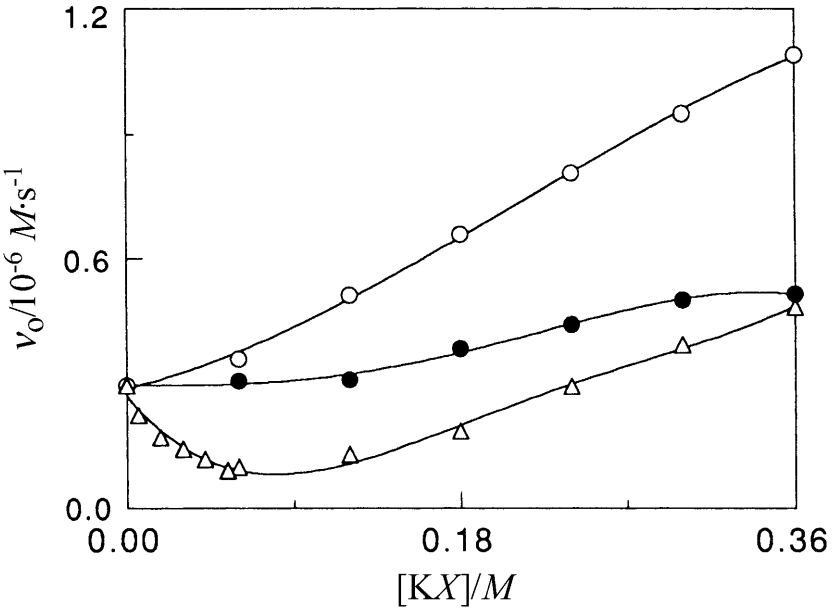

Fig. 10. Dependence of the initial rate on the concentrations of KF (filled circles), KCl (empty circles), and KBr (triangles) at constant ionic strength ($[KX] + [KNO_3] = 0.360\,M$); $[H_2O_2]_0 = 0.392\,M$, $[CuSO_4] = 1.20 \times 10^{-5}\,M$, $[KH_2PO_4] = [K_2HPO_4] = 0.240\,M$, $pH = 6.48 \pm 0.03$, 25.0°C

experimental conditions indicated that Cl^- was more efficient as activator of the catalyst than Br^- at all concentrations (Fig. 9).

The effect of F^- could only be studied at relatively low concentrations (up to $0.360\,M$), because a further increase of its concentration would provoke a considerable increase of the *pH* due to the fact that HF is a much weaker acid than the other hydrogen halides [18a]. At those concentrations, the activating effect of the halide ions followed the sequence $Cl^- > F^- > Br^-$ (Fig. 10). In fact, KBr showed an inhibiting effect at low concentrations followed by an activating effect at higher concentrations. The effect of I^- could not be studied because it reacts with Cu(II) to yield a precipitate of Cu_2I_2 (in addition reacting also with H_2O_2 and with the titrating agent, MnO_4^-).

Mechanism for the parent reaction

The kinetic data so far available on the Cu(II)-catalyzed decomposition of hydrogen peroxide indicate that this reaction follows a rather complex mechanism. Although more experimental information is indeed required to definitively establish the reaction mechanism, a plausible sequence of elementary steps for the reaction in the absence of halide ions might be the following:

$$Cu^{2+} + H_2O_2 \underset{}{\overset{K_I}{\rightleftharpoons}} CuOOH^+ + H^+ \tag{5}$$

$$CuOOH^+ + H_2O_2 \xrightarrow[\text{slow}]{k_{II}} CuOH^{2+} + H_2O + O_2^- \tag{6}$$

$$CuOH^{2+} + H_2O_2 \longrightarrow Cu^{2+} + H_3O^+ + O_2^- \quad (7)$$

$$O_2^- + Cu^{2+} \longrightarrow CuOO^+ \quad (8)$$

$$CuOO^+ \xrightarrow{k_{III}} Cu^+ + O_2 \quad (9)$$

$$Cu^+ + H_2O_2 \longrightarrow Cu^{2+} + OH^- + \cdot OH \quad (10)$$

$$\cdot OH + H_2O_2 \longrightarrow H_3O^+ + O_2^- \quad (11)$$

$$2CuOO^+ + 2H_2O \xrightarrow{k_{IV}} 2Cu^{2+} + H_2O_2 + O_2 + 2OH^- \quad (12)$$

In the first step (Eq. (5)), a hydroperoxocopper(II) ion, $CuOOH^+$, is formed in a reversible reaction. Protein-bound hydroperoxocopper(II) is believed to play an important role as an intermediate in the action of some copper-containing enzymes as dopamine β-monooxygenase [10] and Cu/Zn superoxide dismutase [19]. In the slow step (Eq. (6)), the O–O bond of $CuOOH^+$ is cleaved by reaction with a second H_2O_2 molecule to yield a hydroxocopper(III) ion, $CuOH^{2+}$, and a superoxide radical ion, O_2^-. Cu(III) is known to exist in neutral aqueous solutions in the form of hydroxo complexes, and it is a strong oxidant capable of oxidizing H_2O_2 and other substrates [20]. The oxidative attack of $CuOH^{2+}$ on H_2O_2 (Eq. (7)) yields O_2^-, the latter being coordinated to Cu(II) (Eq. (8)) to form the superoxocopper(II) ion, $CuOO^+$. The homolytic decomposition proposed in Eq. (9) to generate Cu^+ is consistent with that known to occur with a similar superoxo species, the superoxochromium(III) ion $CrOO^{2+}$ [21–23]. Formation of Cu^+ is also consistent with the inhibiting effect caused by Cr(VI) on the Cu(II)/H_2O_2 reaction, probably due to an oxidative scavenging of the intermediate Cu^+ by Cr(VI) [24]. Cu^+ reacts with H_2O_2 in a *Fenton*-like reaction to generate a hydroxyl radical (Eq. (10)) [25, 26]; the latter reacts with hydrogen peroxide to generate O_2^- (Eq. (11)). Although in the gas phase the same reaction generates the protonated form of the radical ($HO_2\cdot$) [27], given that the pK_a value of the latter species in aqueous solution is 4.8 [28], in the nearly neutral media used in the present study the anionic form of the radical (O_2^-) was predominant. Equations (8)–(11) lead to a cyclic decomposition of H_2O_2 by a chain reaction mechanism. Other authors have also proposed chain mechanisms for the Cu(II)/H_2O_2 reaction [29, 30]. Dismutation of $CuOO^+$ is proposed as the chain termination step (Eq. (12)). Equations (8) and (12) are consistent with the known ability of aqueous Cu^{2+} to catalyze the dismutation of superoxide radicals [19, 31].

Assuming that the intermediate $CuOOH^+$ is in *quasi*-equilibrium with the reactants of Eq. (5), whereas the other five intermediates involved ($CuOH^{2+}$, O_2^-, $CuOO^+$, Cu^+, and $\cdot OH$) are in a steady state, the rate law deduced from the proposed mechanism would be

$$v = -\frac{d[H_2O_2]}{dt} = \frac{2K_I k_{II}[Cu^{2+}][H_2O_2]^2}{[H^+]} + 2\left(\frac{K_I k_{II}[Cu^{2+}]}{k_{IV}[H^+]}\right)^{1/2} \cdot k_{III}[H_2O_2] \quad (13)$$

The overall apparent orders predicted by this rate law are intermediary between 1 and 2 for H_2O_2 and between 1/2 and 1 for both Cu^{2+} and OH^-. This is consistent with the kinetic orders slightly below 2 and 1 found for H_2O_2 and OH^-, respectively, in the case of the parent reaction, provided that the first addend in the rate law be predominant over the second. This means that, if the mechanism proposed is correct, the chain length of the reaction is not very high, at least under the experimental

conditions of this study, probably due to the high efficiency of Cu(II) as a scavenger of superoxide radicals [19, 31]. This rate law can also explain two of the three types of v_0 *vs.* $[Cu^{2+}]$ plots observed (Fig. 2), *i.e.* that showing a linear profile and that showing a downward-concave curvature. It cannot explain, however, the type of plot showing an upward-concave curvature. Since the latter type was observed only at high buffer concentration (right below the limit corresponding to precipitation of $CuHPO_4$), it might likely be the consequence of a different reaction pathway taking place on the surface of microcolloidal particles of $CuHPO_4$ [32].

Mechanism for the chloride-activated reaction

Cu(II) forms several different complexes with chloride ions in aqueous solution [33]. Experimental evidences have been reported for the existence of four complexes of general formula $[CuCl_n]^{2-n}$ with $n = 1$, 2, 3, and 4 [34–38]. The complexes for $n = 1$ and 2 show maximum concentrations at $[Cl^-] < 2.64\,M$ [39], which is the upper limit for the range of chloride ion concentrations studied in the present work. Since no maximum was found in the v_0 *vs.* [KCl] plots (Figs. 4–8) it can be concluded that the reactivity of the complexes with $n = 3$ and 4 is higher than that of the complexes with $n = 1$ and 2. Moreover, the rough linearity of these plots suggests that the four complexes react with H_2O_2, the reactivity of each complex increasing markedly as n increases. As $[Cl^-]$ rises, four different zones are passed through. In each zone the predominant chloro complex is $[CuCl_{n-1}]^{3-n}$, but most of the catalyst activation produced by Cl^- in that zone is probably caused by the complex with one more chloro ligand, $[CuCl_n]^{2-n}$, since it has been assumed that the reactivity of $[CuCl_n]^{2-n}$ is much higher than that of $[CuCl_{n-1}]^{3-n}$. In this way, the rough linearity of the v_0 *vs.* [KCl] plots may be easily explained, since in each zone of the $[Cl^-]$ range studied the concentration of the active chloro complex, $[CuCl_n]^{2-n}$, is directly proportional to the product of the concentrations of the predominant chloro complex, $[CuCl_{n-1}]^{3-n}$, and chloride ion.

For the chloride-activated reaction, the following mechanism is proposed:

$$[CuCl_{n-1}]^{3-n} + OH^- \underset{\longleftarrow}{\overset{K_V}{\longrightarrow}} [CuCl_{n-1}(OH)]^{2-n} \tag{14}$$

$$[CuCl_{n-1}(OH)]^{2-n} + Cl^- \underset{\longleftarrow}{\overset{K_{VI}}{\longrightarrow}} [CuCl_n]^{2-n} + OH^- \tag{15}$$

$$[CuCl_n]^{2-n} + H_2O_2 \underset{\longleftarrow}{\overset{K_{VII}}{\longrightarrow}} [CuCl_n(H_2O_2)]^{2-n} \tag{16}$$

$$[CuCl_n(H_2O_2)]^{2-n} + OH^- \underset{\text{slow}}{\overset{k_{VIII}}{\longrightarrow}} [CuCl_n]^{1-n} + O_2^- + H_3O^+ \tag{17}$$

First, the formation of a combined chloro-hydroxo complex (Eq. (14)) is proposed to explain the observation that, although both the parent reaction and the chloride-activated reaction show base catalysis, OH^- is a more efficient catalyst for the former than for the latter. The reason might thus be a competition between OH^- and Cl^- as ligands for Cu(II). Complexation with another Cl^- ligand to yield the n-chloro complex (Eq. (15)) would result in an enhancement of the reactivity with respect to that of the $(n-1)$-chloro complex. Coordination of an H_2O_2 molecule by the n-chloro complex (Eq. (16)) would result in a new complex whose reaction

with OH^- in the slow redox step (Eq. (17)) would yield Cu(I) (as the *n*-chloro complex, $[CuCl_n]^{1-n}$) and a superoxide radical ion. These two intermediates would be involved in a chain reaction mechanism parallel to that of Eqs. (8)–(12), but with Cu^{2+}, $CuOO^+$, and Cu^+ replaced by the corresponding *n*-chloro complexes $[CuCl_n]^{2-n}$, $[CuCl_n(OO)]^{1-n}$, and $[CuCl_n]^{1-n}$.

Assuming that Eqs. (14)–(16) are in *quasi*-equilibrium and that the intermediates involved in the chain reaction mechanism ($[CuCl_n(OO)]^{1-n}$, $[CuCl_n]^{1-n}$, $\cdot OH$, and O_2^-) are in a steady state, the following rate law is obtained for the chloride-activated reaction:

$$v = -\frac{d[H_2O_2]}{dt} = \frac{2K_V K_{VI} K_{VII} k_{VIII} [Cu(II)]_T [H_2O_2][Cl^-][OH^-]}{1 + K_V[OH^-]} + \\ + 2k_{III,c}\left(\frac{K_V K_{VI} K_{VII} k_{VIII} [Cu(II)]_T [H_2O_2][Cl^-][OH^-]}{k_{IV,c}(1 + K_V[OH^-])}\right)^{1/2} \quad (18)$$

where $[Cu(II)]_T$ is the total concentration of Cu(II), assumed to prevail predominantly in the form of the complexes $[CuCl_{n-1}]^{3-n}$ and $[CuCl_{n-1}(OH)]^{2-n}$, whereas $k_{III,c}$ and $k_{IV,c}$ are the rate constants corresponding to Eqs. (9) and (12), respectively, but involving the *n*-chloro complexes.

The rate law deduced can explain the decrease of the kinetic order of H_2O_2 with respect to that corresponding to the parent reaction. Moreover, assuming again that the chain length of the reaction is not very high, the first addend in Eq. (18) would predominate over the second, so that Eq. (18) would be consistent with Eq. (4), the experimental parameters being:

$$a'' = 2K_W K_V K_{VI} K_{VII} k_{VIII} [Cu(II)]_T [H_2O_2] \quad (19)$$

and

$$b'' = K_W K_V \quad (20)$$

where K_W is the ionic product of water. The value deduced from Eq. (20) for the equilibrium constant corresponding to Eq. (14) is $K_V = (6.2 \pm 0.2) \times 10^7 M^{-1}$.

It has been reported that the rate of oxidation of Fe(II) by H_2O_2 is increased by the presence of Cl^- [40]. This contrasts with the decreasing effect of Cl^- on the rate of oxidation of Cu(I) by H_2O_2, attributed to a decrease of the reducing power of Cu(I) as the extent of coordination of chloride ions increases [41]. This fact, as well as the finding in the present work that Cl^- activates the catalytic power of Cu(II) for the decomposition of H_2O_2, can both be explained if it is accepted that coordination of the chloride ions stabilizes Cu(I) more than Cu(II). Thus, an increase of the number of chloro ligands (*n*) bound to Cu(II) would result in an increase of its tendency to be reduced to Cu(I) and, therefore, in an increase of the rate constant k_{VIII} corresponding to the slow step (Eq. (17)). This would also explain the low activation energy associated to the chloride-activated reaction as compared to that associated to the parent reaction.

Inhibition by phosphate ions

The rates of both the parent reaction and the chloride-activated reaction decrease with increasing phosphate buffer concentration (Table 2 and Fig. 6). This contrasts

with the accelerating effect produced by phosphate ions on the rate of the reaction between Cr(VI) and H_2O_2 [42]. In the case of the Cu(II)/H_2O_2 reaction, the inhibiting effect caused by the buffer suggests that phosphate ions might compete with H_2O_2 and Cl^- as ligands for Cu(II).

Inhibition by bromide ions

The inhibiting effect provoked by Br^- at low concentrations (Fig. 10) may be caused by participation of that ion in the termination of the chain reaction:

$$\cdot OH + Br^- \rightarrow OH^- + Br\cdot \quad (21)$$

$$2Br\cdot \rightarrow Br_2 \quad (22)$$

Here, a very reactive free radical (·OH) is replaced by a less reactive one (Br ·) that can accumulate to disappear *via* a bimolecular recombination. The predominance of the inhibition effect at low Br^- concentration and of the catalyst activation effect at high Br^- concentration explains the S-shaped profile of the v_0 *vs.* [KBr] plot (Fig. 9). Inhibition was observed only in the case of Br^-, consistent with the fact that this is the most oxidizable ion of the three halides studied as indicated by the corresponding standard X_2/X^- (with $X = F, Cl, Br$) reduction potentials [18b].

Biological implications

Cu(II) is present in human cells in concentrations that usually are in the micromolar range [8], whereas the concentration of H_2O_2 might be an order of magnitude higher at the most [14, 43]. According to the results of this investigation, the rate of the intracellular Cu(II)-catalyzed decomposition of hydrogen peroxide at physiological *pH* would be rather low. However, the destruction of H_2O_2 through a nonenzymatic process is likely to involve the formation of free radicals, and the generation of even a few radicals per second might be very noxious for the cell [2]. As seen in this work, the presence of halide (especially, Cl^-) ions inside the cell enhances the catalytic power of Cu(II) for the decomposition of H_2O_2, although protein-bound Cu(II) might presumably be much less reactive than free Cu(II) [19].

The possible participation of the intermediates Cu^+, ·OH, and O_2^- in the mechanism would be of some biological relevance. Due to the high affinity of *DNA* for Cu^+ [14], the Cu(II)/H_2O_2 reaction could lead to *DNA* lesions when occurring in the vicinity of chromosomes. Moreover, the reactive oxygen species ·OH and O_2^- may cause oxidative stress, eventually leading to aging and carcinogenesis [1–3] as well as cell apoptosis [44].

Experimental

The solvent employed was water previously purified by deionization, distillation, and circulation through a Millipore system. Hydrogen peroxide (30% additive-free aqueous solution) was obtained from Fluka, all other chemicals ($CuSO_4 \cdot 5H_2O$, KF, KCl, KBr, KNO_3, $NaClO_4 \cdot H_2O$, H_3PO_4, KH_2PO_4, $K_2HPO_4 \cdot 3H_2O$) from Merck. The *pH* measurements were done with a Metrohm 605 pH-meter provided with a glass-calomel combined electrode. The UV/Vis spectra were recorded with a Shimadzu UV-2101PC spectrophotometer.

The reaction was followed by taking aliquots from the thermostatted reacting mixture at appropriate intervals and titrating them with $KMnO_4$ (1.00×10^{-2} M) in the presence of excess H_2SO_4. A Brand Bürette Digital II (accuracy $\pm 0.01\,cm^3$) was used for the titrations. In the experiments performed at high Br^- concentration the titration results had to be corrected because a small fraction ($< 1\%$) of the permanganate added was used to oxidize Br^- rather than H_2O_2. For that purpose, the amount of bromine liberated was determined by a spectrophotometric measurement of its absorbance at 352 nm.

References

[1] Sagripanti JL, Kraemer KH (1989) J Biol Chem **264**: 1729
[2] Halliwell B, Gutteridge JMC (1990) Methods Enzymol **186**: 1
[3] Toyokuni S (1996) Free Radic Biol Med **20**: 553
[4] Cortopassi G, Wang E (1995) Biochim Biophys Acta **1271**: 171
[5] Slyshenkov VS, Moiseenok AG, Wojtczak L (1996) Free Radic Biol Med **20**: 793
[6] Bohr V, Vilhelm A, Dianov GL (1999) Biochimie **81**: 155
[7] Hanna MG, Nelson IP (1999) Cell Mol Life Sci **55**: 691
[8] Meggers E, Holland PL, Tolman WB, Romesberg FE, and Schultz PG (2000) J Am Chem Soc **122**: 10714
[9] Marzotto A, Clemente DA, Zampiron A, Carrara M (2000) Nucleosides Nucleotides Nucleic Acids **19**: 1311
[10] Klinman JP (1996) Chem Rev **96**: 2541
[11] Solomon EI, Sundaram UM, Machonkin TE (1996) Chem Rev **96**: 2563
[12] Chen P, Fujisawa K, Solomon EI (2000) J Am Chem Soc **122**: 10177
[13] Mahadevan V, Henson MJ, Solomon EI, Stack TDP (2000) J Am Chem Soc **122**: 10249
[14] Prütz WA (1994) Biochem J **302**: 373
[15] Prütz WA (1996) J Biochem Biophys Methods **32**: 125
[16] Ohta Y, Shiraishi N, Nishikawa T, Nishikimi M (2000) Biochim Biophys Acta **1474**: 378
[17] Livingston RS, Bray WC (1925) J Am Chem Soc **47**: 2069
[18] Weast RC (ed) (1977) Handbook of Chemistry and Physics. CRC Press, Cleveland, (a) p D-151, (b) p D-141
[19] Holm RH, Kennepohl P, Solomon EI (1996) Chem Rev **96**: 2239
[20] Meyerstein D (1971) Inorg Chem **10**: 638
[21] Brynildson ME, Bakac A, Espenson JH (1987) J Am Chem Soc **109**: 4579
[22] Bakac A, Won TJ, Espenson JH (1996) Inorg Chem **35**: 2171
[23] Perez-Benito JF, Arias C (1998) J Phys Chem A **102**: 5837
[24] Perez-Benito JF, Arias C (1999) New J Chem **23**: 945
[25] Masarwa M, Cohen H, Meyerstein D, Hickman DL, Bakac A, Espenson JH (1988) J Am Chem Soc **110**: 4293
[26] Eberhardt MK, Ramirez G, Ayala E (1989) J Org Chem **54**: 5922
[27] Lamb JJ, Molina LT, Smith CA, Molina MJ (1983) J Phys Chem **87**: 4467
[28] Fridovich I (1972) Acc Chem Res **5**: 321
[29] Sychev AY, Duka GG (1983) Zh Fiz Khim **57**: 2209
[30] Ernestova LS, Skurlatov YI (1984) Zh Fiz Khim **58**: 2358
[31] Espenson JH (1995) Chemical Kinetics and Reaction Mechanisms. McGraw-Hill, New York, p 105
[32] Ernestova LS, Skurlatov YI (1984) Zh Fiz Khim **58**: 739
[33] Cotton FA, Wilkinson G (1988) Advanced Inorganic Chemistry. Wiley, New York, p 767
[34] Schwing-Weill MJ (1973) Bull Soc Chim Fr 823
[35] Khan MA, Schwing-Weill MJ (1976) Inorg Chem **15**: 2202
[36] Ashurst KG, Hancock RD (1981) J Chem Soc Dalton Trans 245

[37] Bjerrum J, Skibsted LH (1986) Inorg Chem **25**: 2479
[38] Ramette RW (1986) Inorg Chem **25**: 2481
[39] Ramette RW, Fan G (1983) Inorg Chem **22**: 3323
[40] Po HN, Sutin N (1968) Inorg Chem **7**: 621
[41] Nicol MJ (1982) S Afr J Chem **35**: 77
[42] Perez-Benito JF, Arias C (1997) J Phys Chem A **101**: 4726
[43] Itoh M, Nakamura M, Suzuki T, Kawai K, Horitsu H, Takamizawa K (1995) J Biochem **117**: 780
[44] Burkitt MJ, Milne L, Nicotera P, Orrenius S (1996) Biochem J **313**: 163

Received March 27, 2001. Accepted (revised) May 25, 2001.